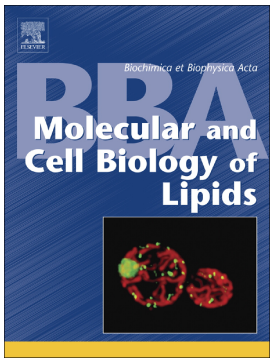

Determining the target of membrane sterols on voltage-gated potassium channels

Florina Zakany, Pal Pap, Ferenc Papp, Tamas Kovacs, Peter Nagy, Maria Peter, Lajos Szente, Gyorgy Panyi, Zoltan Varga

PII: S1388-1981(18)30307-X
DOI: https://doi.org/10.1016/j.bbalip.2018.12.006
Reference: BBAMCB 58397

To appear in: *BBA - Molecular and Cell Biology of Lipids*

Received date: 28 September 2018
Revised date: 30 November 2018
Accepted date: 12 December 2018

Please cite this article as: Florina Zakany, Pal Pap, Ferenc Papp, Tamas Kovacs, Peter Nagy, Maria Peter, Lajos Szente, Gyorgy Panyi, Zoltan Varga , Determining the target of membrane sterols on voltage-gated potassium channels. Bbamcb (2018), https://doi.org/10.1016/j.bbalip.2018.12.006

Determining the target of membrane sterols on voltage-gated potassium channels

Florina Zakany[a], Pal Pap[a,b], Ferenc Papp[a,b], Tamas Kovacs[a], Peter Nagy[a], Maria Peter[c], Lajos Szente[d], Gyorgy Panyi[a,b], Zoltan Varga[a,b]

[a] Division of Biophysics, Department of Biophysics and Cell Biology, Faculty of Medicine, University of Debrecen, Debrecen, Egyetem ter 1., H-4032, Hungary
[b] MTA-DE-NAP B Ion Channel Structure-Function Research Group, RCMM, University of Debrecen, Debrecen, Egyetem ter 1., H-4032, Hungary
[c] Institute of Biochemistry, Biological Research Center of the Hungarian Academy of Sciences, Szeged, Temesvari Krt. 62., H-6726, Hungary
[d] CycloLab Cyclodextrin R & D Laboratory Ltd., Budapest, Illatos u. 7, H-1097, Hungary

Corresponding author: Zoltan Varga, Division of Biophysics, Department of Biophysics and Cell Biology, Faculty of Medicine, University of Debrecen, Debrecen, Egyetem ter 1., H-4032, Hungary, email: veze@med.unideb.hu

Abstract

Cholesterol, an essential lipid component of cellular plasma membranes, regulates fluidity, mechanical integrity, raft structure and may specifically interact with membrane proteins. Numerous effects on ion channels by cholesterol, including changes in current amplitude, voltage dependence and gating kinetics, have been reported. We have previously described such changes in the voltage-gated potassium channel $K_v1.3$ of lymphocytes by cholesterol and its analog 7-dehydrocholesterol (7DHC). In voltage-gated channels membrane depolarization induces movement of the voltage sensor domains (VSD), which is transmitted by a coupling mechanism to the pore domain (PD) to open the channel. Here, we investigated whether cholesterol effects were mediated by the VSD to the pore or the PD was the direct target. Specificity was tested by comparing $K_v1.3$ and $K_v10.1$ channels having different VSD-PD coupling mechanisms. Current recordings were performed with two-electrode voltage-clamp fluorometry, where movement of the VSDs was monitored by attaching fluorophores to external cysteine residues introduced in the channel sequence. Loading the membrane with cholesterol or 7DHC using methyl-β-cyclodextrin induced changes in the steady-state and kinetic parameters of the ionic currents while leaving fluorescence parameters mostly unaffected in both channels. Non-stationary noise analysis revealed that reduction of single channel conductance rather than that of open probability caused the observed current decrease. Furthermore, confocal laser scanning and stimulated emission depletion microscopy demonstrated significant changes in the distribution of these ion channels in response to sterol loading. Our results indicate that sterol-induced effects on ion channel gating directly target the pore and do not act via the VSD.

Keywords: cholesterol; ion channel gating; voltage-sensor; pore domain; $K_V1.3$; $K_V10.1$

1. Introduction

Composition of the membrane lipid environment affects the function of the embedded ion channels. These effects may occur via nonspecific routes by influencing membrane properties like fluidity, lateral forces or curvature, but can also act more specifically via the reorganization of lipid domains, alteration of local electric fields or even through selective lipid-channel interactions where lipids actively participate in gating [1-3].

Cholesterol, an essential component of the plasma membrane, is also known to interact with ion channels. Besides structurally stabilizing the membrane, cholesterol is involved in various membrane-associated signaling cascades, the regulation of fluidity, lipid microdomain structure and the operation of transmembrane proteins. Modulatory effects by cholesterol on a variety of ion channels with different ion selectivities, gating mechanisms and tissue distribution have been reported [4]. There is considerable heterogeneity in these effects: enrichment of the membrane with cholesterol resulted in altered open probability, single channel conductance, or kinetic and equilibrium parameters of the ionic current [5-10]. Contradicting reports about similar ion channels are not rare either.

Most often channel activity is suppressed by cholesterol enrichment or enhanced by cholesterol depletion of the membrane, as was observed for several K^+ channels [8,10-14], voltage-gated Na^+ channels [15], as well as volume-regulated anion channels [16]. In some other channels, however, the opposite was reported: depletion of membrane cholesterol inhibited epithelial Na^+ channels (eNaC) [17] and transient receptor potential (Trp) channels [18,19].

Based on the conclusions of these studies two possible mechanisms have emerged to explain cholesterol effects on channel gating: specific interaction with the channel via a binding site; or an indirect effect through changes in the physical parameters of the membrane (e.g. stress, fluidity, curvature), and of course, the most likely scenario is a combination of these mechanisms.

Early descriptions of cholesterol effects [8,20-22] proposed an indirect mechanism, according to which a channel going through a conformational change distorts the adjacent lipid bilayer and requires more energy for this movement if the viscosity and rigidity of its environment is increased by cholesterol. On the other hand, the observation that inwardly-rectifying K^+ channels are sensitive to the chiral nature of sterol analogues supports the view that cholesterol-sensitivity may arise from specific sterol-protein interactions and is not simply related to sterol content [23,24].

Being membrane proteins, ion channels may associate with lipid rafts, which can alter their function. Lipid rafts are defined as membrane microdomains with a specialized lipid composition with elevated cholesterol and sphingolipid content and lipids arranged in a liquid ordered state. Rafts are more resistant to detergents and enclose specific proteins often to enhance intermolecular interactions. [25].

Numerous reports describe the association of certain K_v channels with rafts or the exclusion of others [5,6,9,10,26,27]. Cyclodextrins are often employed to manipulate the amount of cholesterol in the cell membrane. For selective removal of cholesterol from the membrane methyl-β-cyclodextrin (MβCD) is used most frequently [28,29]. Preloaded with cholesterol or even 7-dehydrocholesterol (MβCD/C and MβCD/7DHC), it can also be applied to enrich the membrane with sterols. Thus, disruption or reorganization of the raft arrangement in the membrane can be

achieved and its consequences on ion channel function observed. However, cyclodextrins do not selectively remove cholesterol from rafts [30], so altered channel function does not necessarily result from raft rearrangement. The affinity of channels for rafts may show high variability, and can be influenced by the precise membrane lipid composition, including the amount of cholesterol, the association of the channel with scaffolding proteins or accessory subunits [31,32]. As a result, raft association is likely to depend on the cell type expressing a particular K_v channel [33,34].

In this study we investigated membrane sterol effects on voltage-gated K^+ channels, which comprise a large number of channels with a similar structure and fundamental gating mechanism, yet very broad tissue distribution and differing gating properties [35]. The major K^+ channel of human lymphocytes, $K_v1.3$ and a channel mostly found in the brain and several tumor types, $K_v10.1$ were studied [36,37].

K_v channels are made up of four (often identical) subunits, which together form four voltage-sensor domains (VSD) and a central pore domain (PD) [38] (**Fig. 1 A**). Each subunit contains six transmembrane segments, of which the first four (S1-S4) form the VSD in each subunit and the S5-S6 segments along with the linker connecting them from all four subunits together form the central pore domain [39,40] (**Fig. 1 B**). In response to depolarization of the membrane, the VSDs are activated, which means a conformational change involving the outward movement of the highly charged S4 segments [41,42]. The conformational change of the pore leading to channel opening occurs at the intracellular end of the S6 segments and is mainly voltage-independent. The mechanism that transfers the motion of the VSDs to the pore to realize voltage-gated opening is called coupling, which relies on the rigid connection of the domains by the S4-S5 linker acting as a lever in some K_v channels and on less well-defined contact points between helices establishing a looser inter-domain connection in others [43-45]. $K_v1.3$ employs the former structure, which accomplishes a tight "linear" coupling between the VSD and the PD, whereas in members of the *ether-à-go-go* (*eag)* family, such as $K_v10.1$, coupling is looser between the two functional domains [45,46]. When the S4-S5 linker "lever" is cut or deleted, $K_v10.1$ still performs voltage-dependent gating, probably through inter-helix interactions [47]. $K_v10.1$ has three cytoplasmic domains, a Per-ARNT-Sim (PAS) domain at the N-terminus, a C-terminal C-linker domain, and a cyclic nucleotide-binding homology domain (CNBHD), which can also modify the gating of the channel [45].

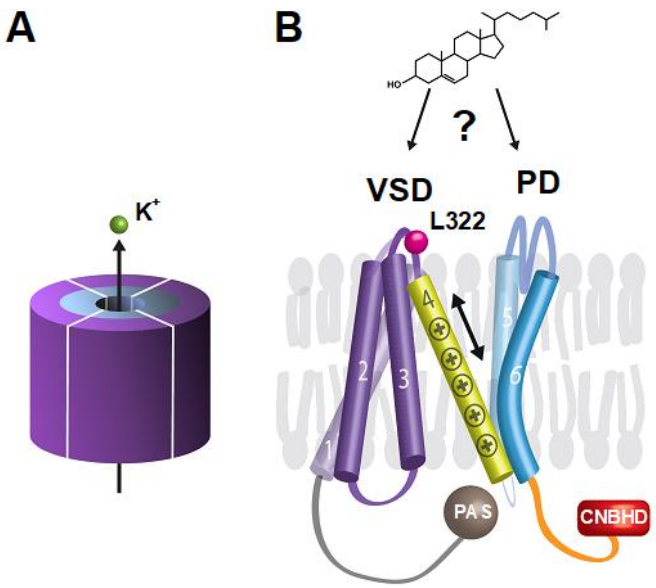

Fig. 1 Basic structure of K_v10.1 channels

The members of the voltage-gated potassium channel family (K_v) are built up by four identical subunits (**A**). The potassium ion (K^+, green) conducting pore is formed by the pore domains (PD, blue) while the voltage-sensor domains (VSD, purple) are responsible for monitoring the actual membrane potential. Each subunit consists of six transmembrane helices which are connected via intra- or extracellular loops. Panel **B** represents the basic structure of one subunit from lateral view in closed conformation. The S1-S4 helices form the VSD, while the S5 and S6 form the PD. The S4 helix contains positively charged amino acids (five in K_v10.1) that are responsible for voltage-sensing. In response to membrane depolarization the S4 helix (yellow) moves upward (arrow), and this movement is transmitted to the pore domain permitting potassium ions flow through the channel. Pink sphere on the S3-S4 linker represents the location of the cysteine mutation for labeling. Members of the *eag* family, including K_v10.1 have two intracellular domains that are functionally distinct from other K_v channels including K_v1.3. The N-terminal Per-ARNT-Sim (PAS) domain (gray) interacts with the S4 helix, thus determining the activation kinetics of the ionic current. Via the C-linker (orange), the S6 helix proceeds to the cyclic nucleotide-binding homology (CNBHD) domain (red), which is also an important gating modulator. The major goal of the study was to determine the intramolecular target (VSD or PD) of membrane sterols.

Considering that the K_v family includes about 40 members, the amount of data available about their interaction with cholesterol is rather limited. Effects of cholesterol depletion on K_v1.5, K_v2.1, K_v1.3 and K_v11.1 gating and raft-partitioning were described in different systems, while for several other K_v types only cholesterol effects on the association between the channels and rafts was studied, with the obtained results being just as diverse as for all other channels in general [5,6,14,48-50].

K_v10.1, one of the channels investigated here, can associate with or be excluded from rafts. Its distribution between the two regions is determined by cholesterol content and interactions with the cytoskeleton. Depletion of cholesterol resulted in elevated K_v10.1 current density while other gating parameters were unaffected [27].

We and others have previously studied the effect of cholesterol on the gating of K_v1.3 channels [9,10,51], but due to the differences in expression systems, MβCD incubation periods and

concentrations, the results are inconsistent, often conflicting. In our system, *in vitro* cholesterol loading of human lymphocytes by MβCD/C decreased the current density, shifted the voltage-dependence and slowed the kinetics of $K_v1.3$ channels [10]. We have found similar effects of 7DHC on $K_v1.3$ gating [52], a precursor of cholesterol, which only differs from cholesterol by the presence of an extra double bond. 7DHC is enriched in the cell membrane of patients suffering from Smith-Lemli-Opitz (SLO) syndrome [53]. Voltage-dependence was shifted and activation kinetics were slowed in channels from SLO cells and also from cell lines loaded with 7DHC. Current density was also reduced by 7DHC enrichment in the latter, but not the former population. Although some conflicting results with cholesterol depletion are apparent in these previous reports on $K_v1.3$, they all shared the common findings of $K_V1.3$ localizing to rafts and that manipulation of raft structure alters $K_v1.3$ gating. These indicate an intimate relationship of the channel with cholesterol.

Voltage-dependent gating of ion channels comprises multiple conformational transformations of the protein in response to a change in membrane potential. Membrane cholesterol may influence the rearrangement of either of the main functional domains. Our aim in this study was to determine if the observed changes in the gating of K_v channels originated from sterol effects on the VSD, which propagate downstream or the coupling machinery and / or the pore domain are directly modulated. We employed the two-electrode voltage-clamp fluorometry technique, which allows simultaneous observation of the pore domain by measuring the ionic current and the movement of the VS domains via the fluorescence signal of an attached fluorophore from the same channel population. Voltage-dependent steady-state and kinetic parameters of VSD activation and pore opening were compared in two K_v channels with different coupling mechanisms in control and sterol-enriched membranes to learn about the target and the specificity of the sterol modulation.

2. Materials and Methods

2.1 Molecular biology, expression systems

The human $K_v1.3$ (KCNA3, Uniprot B2RA23) A309C channel containing a cysteine mutation in the S3-S4 linker was constructed via site-directed mutagenesis (QuikChange; Agilent, Santa Clara, CA) in a pBSTA vector and the mutation was verified by sequencing. The human $K_v10.1$ (KCNH1, Isoform 1, Uniprot O95259-2) L322C mutant in pSGEM vector was a kind gift of L. A. Pardo (Max Planck Institute, Göttingen, Germany). Plasmids were linearized with HindIII ($K_v1.3$) or NheI ($K_v10.1$) and transcribed to RNA with the Invitrogen mMESSAGE mMACHINE T7 Transcription Kit (ThermoFisher, Waltham, MA).

Xenopus laevis oocytes for two-electrode voltage-clamp fluorometry experiments were purchased from EcoCyte Bioscience (Dortmund, Germany). Oocytes were injected with 30-50 nl of RNA at a concentration of ~1 µg/µl and incubated at 18°C for 1–3 days in ND93 containing 93 mM NaCl, 5 mM KCl, 1.8 mM $CaCl_2$, 1 mM $MgCl_2$, 5 mM HEPES and 50 mg/l Gentamycin, pH 7.4. Chemicals used for the preparation of the solutions were purchased from Sigma-Aldrich (St. Louis, MO).

For microscopy experiments the human embryonic kidney cell line HEK-293 was obtained from the American Type Culture Collection (ATCC, Manassas, VA) and grown according to its specifications. HEK-293 cells grown on 8-well chambered coverglass were transfected with 0.25 μg DNA/well wild-type $K_v1.3_{FLAG}$ (provided by Peter Hajdu, University of Debrecen, Hungary), wild-type $K_v10.1_{FLAG}$ (in pCMV6 plasmid, OriGene RC215104) or GFP-GPI encoding plasmids using Lipofectamine2000 (ThermoFisher) at a lipid to DNA ratio of 2:1 (μl/μg). The GFP-GPI plasmid was a kind gift from Jennifer Lippincott-Schwartz (NIH, Bethesda, MD). Channels were transiently expressed in the cells for 12-36 hours after transfection.

2.2 Cell membrane sterol modulations

Cholesterol (Sigma-Aldrich), NBD-cholesterol (Avanti Polar Lipids, Alabaster, AL) or 7-dehydrocholesterol (Sigma-Aldrich) loading was performed with custom synthetized sterol-methyl-beta-cyclodextrin (MβCD) complexes (CycloLab Cyclodextrin R&D Laboratory, Budapest, Hungary), with loading solutions containing 195μM sterol at room temperature for 60 min before the electrophysiological or microscopic experiments. For electrophysiology the sterol-MβCD complexes were dissolved in ND93, or for microscopy in the extracellular recording solution used in patch-clamp measurements (see below). For both cases after the incubation oocytes and cells were extensively washed with ND93 or the extracellular recording solution, respectively.

2.3 Two-electrode voltage-clamp fluorometry (TEVCF)

For TEVCF recordings oocytes were labeled for 30 min on ice with 10 μM of 2-((5(6)-tetramethylrhodamine)carboxylamino)ethyl methanethiosulfonate (TAMRA-MTS, Toronto Research Chemicals, Toronto, ON, Canada), diluted in a depolarizing solution (110 mM KCl, 1.5 mM $MgCl_2$, 0.8 $CaCl_2$, 0.2 EDTA, 10 HEPES, pH 7.1). After labeling, oocytes were extensively washed in ND93 solution and stored in the dark on ice during the course of the experiment. During the experiments the extracellular recording solution was ND93, the intracellular solution was a 3M KCl solution.
TEVCF recordings were collected with an Oocyte Clamp OC-725C amplifier (Warner Instruments, Hamden, CT). Fluorescence signals were acquired through a 40×, 0.8-NA CFI Plan Fluor Nikon fluorescence water-immersion objective on a Nikon Eclipse FNI microscope (Nikon, Tokyo, Japan) and a photodiode (PIN-040A; United Detector Technology, OSI Optoelectronics, Hawthorne, CA). TAMRA-MTS signals were recorded using a 545/25 excitation filer, a 565LP dichroic mirror and a 605/70 emission filter. The signal from the photodiode was acquired by an Axopatch 200A amplifier and a Digidata-1550 digitizer controlled by pClamp10 (Molecular Devices, San Jose, CA). Illumination was provided by a green LED (530 nm), M530L2-C1 from ThorLabs (Newton, NJ). Fluorescence traces represent single recordings (without averaging) and were filtered with a Gaussian filter.

2.4 Patch-clamp recordings

Patch-clamp recordings determining single channel properties were performed on mechanically devitellinzed oocytes using outside-out configuration. The standard intracellular solution contained 105 mM KF, 35 mM KCl, 10 mM EGTA and 10 mM HEPES at pH 7.36–7.38. Standard extracellular solution was 150 mM NaCl, 5 mM KCl, 1.5 mM $CaCl_2$, 1 $MgCl_2$ mM and 10 mM HEPES, pH 7.36–7.38. Measurements were carried out by using Axopatch 200B and Multiclamp 700B amplifiers connected to a personal computer using Axon Digidata 1550 data acquisition hardware (Molecular Devices).

2.5 Confocal laser scanning and stimulated emission depletion (STED) microscopy

For microscopic analysis, lipid rafts of HEK-293 cells were labeled with two different methods. First, GM1-enriched membrane rafts were labeled by 8 μg/ml AlexaFluor647-tagged subunit B of cholera toxin (CTX-B) (ThermoFisher) for 20 min on ice to prevent internalization of CTX-B. Second, for labeling lipid rafts with GFP-GPI, cells were transfected with a GFP-GPI plasmid, as described previously [54].

For labeling ion channels, cells expressing $K_v1.3_{FLAG}$ or $K_v10.1_{FLAG}$ were incubated in the presence of 2 μg/ml anti-FLAG M2-Cy3 antibodies (Sigma-Aldrich) for 30 min on ice. Since the FLAG tag on $K_v10.1$ is localized on the intracellular side, labeling of these channels was carried out after fixation of the cells in 3.7% formaldehyde in PBS containing 0.1% BSA and 0.1% Triton X-100.

After labeling of sterol-treated or control cells, images were taken from the flat cell membrane region attached to the coverslip with an LSM880 confocal laser scanning microscope (Carl Zeiss AG, Jena, Germany). NBD, GFP, Cy3 and AlexaFluor647 were excited at 458 nm, 488 nm, 543 nm and 633 nm, respectively, and their emitted intensities were detected in the wavelength ranges of 482-696 nm, 493-598 nm, 548-629nm, and 638-756 nm, respectively.

For STED microscopy measurements, cells expressing $K_v1.3_{FLAG}$ were labeled with 2 μg/ml anti-FLAG M2 (Sigma-Aldrich) for 30 min at room temperature, which was followed by an incubation with 8 μg/ml AlexaFluor594-CTX-B (ThermoFisher) and StarRed-GAMIG (Abberior, Göttingen, Germany) for 30 min on ice.

Images were acquired from the flat cell membrane region attached to the coverslip with an Olympus BX53 microscope equipped with a STED module (Abberior) and an Olympus 100x/1.4 objective using excitation at 594 and 640 nm and a STED laser beam at 775 nm. Detection bands were 608-627 nm and 650-700 nm for AlexaFluor594 and StarRed, respectively.

2.6 Data analysis

Electrophysiological data analyses were performed using Clampfit (v10; Molecular Devices), SigmaPlot (v10.; Systat Software, San Jose, CA) and Excel (Microsoft, Redmond, WA).

Current and fluorescence signals were recorded at 5 kHz and low-pass filtered at 1 kHz. The magnitude of the fluorescence signals was expressed as $\Delta F/F$ in percentage, where ΔF is the change in the signal amplitude, and F is the baseline fluorescence level at the time of the signal. To correct for photobleaching, the baseline fluorescence trace, which has no change in voltage, was subtracted from all other traces. F_{norm}-V values of $K_v1.3$ 309C were obtained from the

steady-state components of the fluorescent signals, normalized to the maximum intensity and plotted as a function of test potential. MTS-TAMRA labeled K_v10.1 322C exhibits a complex fluorescent signal that can be divided into hyperpolarized (from -180 to -90 mV) and depolarized (from -80 to +60 mV) components. The hyperpolarized signals had two components of the same polarity and were analyzed similarly to K_v1.3 signals. The depolarized signals had two components of opposite polarities. To determine the absolute value of the signal, the second component was added to the first with an inverted polarity.

I-V curves were constructed by plotting leak-corrected peak currents as a function of test potential. $V_{1/2}$ and k parameters of K_v1.3 309C and K_v10.1 322C G-V curves were determined by fitting the

$$I = V \times G_{max} \times (1-e^{-(V-E_{rev})/25})/[(1-e^{-(V/25)}) \times (1/(1+e^{-(V-V_{1/2})/k}))]$$

equation to I-V curves, which combines Goldman-Hodgkin-Katz rectification with Boltzmann voltage-dependence. Here V and I are the voltage and the current, respectively, and the free parameters are G_{max}, the maximum conductance, E_{rev} the reversal potential, $V_{1/2}$ and k the half-activation voltage and slope factor of the Boltzmann function, respectively. Then normalized G values at given test potentials were calculated with $G(V) = 1/(1+e^{-(V-V_{1/2})/k})$ for each cell.

To determine the activation time constants for ionic currents a single exponential ($I = I_0 \times (1-e^{-t/\tau}) + C$) function was fitted to the rising phase of the traces. For fluorescent signals double exponential functions ($I = I_{0f} \times (1 - e^{-t/\tau_f}) + I_{0s} \times (1 - e^{-t/\tau_s}) + C$) were applied to determine fast (τ_f) and slow (τ_s) time constants.

To construct steady-state inactivation curves the fraction of non-inactivated channels at each voltage was calculated as I/I_{-120}, where I is the peak current evoked by the depolarization from a given prepulse potential, whereas I_{-120} is the peak current evoked by identical depolarization from the holding potential of −120 mV.

Steady-state voltage dependence curves (F_{norm}-V, SSI) were quantified by fitting a Boltzmann function: $y = 1/(1 + e^{-(V-V_{1/2})/k})$ and determining $V_{1/2}$ and k from the fits.

To investigate the Cole-Moore shift of K_v10.1 channels a 500 ms long depolarizing pulse was applied to +40 mV following a 10-s-long prepulse to potentials ranging from -160 mV or -60 mV. To determine the activation time constants of the ionic currents a single exponential function was fitted to currents evoked from each prepulse potential. The first sigmoidal phase of the currents was excluded from the fitting interval.

For determining current decrease caused by sterol loading in TEVCF measurements, leak corrected peak currents evoked by a +40 mV (for K_v1.3) or +60 mV (for K_v10.1) depolarizing pulse were pooled for each day for the control, cholesterol, and 7DHC loaded oocytes, respectively and then normalized to the mean of the control peaks. Thus we obtained a relative current amplitude for each day and SEMs originate from the day-to day variability of the normalized peak amplitudes.

For non-stationary noise analysis, outside-out patches were excised from oocytes and 200 ms long depolarizing pulses were applied to +50 mV 200 times every 2 seconds from a holding potential of -100 mV. Traces significantly deviating from the mean due to rundown were omitted from the analysis. For each time point along the trace (isochrones) the mean current <I> of the traces and the variance of the current, σ_I^2 were calculated. Then σ_I^2 was plotted as a function of

<I>, yielding a parabola with the equation: $\sigma_I^2 = i <I> - (<I>^2 / N)$, where i is the single channel current and N is number of channels in the patch [55]. Single channel current was determined from the first derivative of the parabola at the roots, single channel conductance was calculated as $i / (V-E_{rev})$, where V is the applied test potential and E_{rev} is the reversal potential of the K^+ current. Open probability was calculated as the maximum of <I> divided by the positive root of the parabola, iN, the theoretical maximum of <I> occurring at $P_o = 1$.

After labeling of HEK-293 cells and image acquisition using confocal laser scanning or STED microscopy, the extent of co-localization of ion channels and lipid rafts was determined as described previously [54,56]. Briefly, the Pearson correlation coefficients between the intensities of the raft marker, the antibodies against ion channels and in certain cases the fluorescently labeled cholesterol were calculated. During image processing calculations were carried out in cell membrane pixels selected manually with a "cell mask". The Pearson coefficients were determined from pixelwise intensity data of individual cells with a custom-written algorithm under Matlab (Mathworks, Natick, MA). To rule out the accidental positive correlation, we determined the 95% confidence interval of the coefficient assuming no correlation between the analyzed parameters according to the method of Costes [57]. As a positive control, the correlation coefficient between two known lipid raft markers was also calculated.

All electrophysiological experiments were carried out on oocytes originating from at least 3 different frogs. Microscopy data were obtained by analyzing three or more independent experiments.

Reported errors are SEM, numbers of cells (n) involved in the given analysis are shown in the text. P values were calculated based ANOVA analysis followed by Tukey's HSD test. Differences were considered significant (asterisk, *) when $p<0.05$.

3. Results

3.1 Sterol effects on voltage-dependent steady-state parameters of $K_v1.3$

Our previous results on the sterol-sensitivity of $K_v1.3$ channel gating showed that cholesterol or 7DHC-enrichment of the membrane reduced the whole-cell current, caused a right-shift of the G-V curve and slowed activation kinetics in human lymphocytes and CHO cells [10,52]. We confirmed all these observations in the *Xenopus* oocyte expression system with wild-type $hK_v1.3$ channels indicating that despite the differences in membrane composition, the *Xenopus* system is a valid model for such protein-membrane interactions in mammalian cells (**Suppl. 1**).

In order to study voltage sensor movements in $hK_v1.3$ channels by VCF, a cysteine must be introduced in the external S3-S4 linker of the channel for fluorophore labeling. Since no previous reports on $K_v1.3$ VCF mutants existed, several residues in the linker were tested to find the optimal position. An Ala→Cys mutation at position 309 close to the top of S4 proved to be the most suitable choice for VCF as it gave large voltage-dependent fluorescence signals. The A309C mutant conserved the basic gating properties of $K_v1.3$, such as the steepness of the voltage-dependence and activation kinetics (**Fig. 2 A-C**, **Fig. 3 A**, **Suppl. 1**), although it shifted the G-V curve similarly to most VCF cysteine-mutations. Labeling by MTS-TAMRA yielded

fluorescence signals superior to those of Alexa488 and TMRM (data not shown). The $hK_v1.3$ has no native extracellular cysteines, which precludes non-specific labeling of the channel. Since the majority of the manuscript is about the cysteine-containing channels used for electrophysiological experiments, $K_v1.3$ and $K_v10.1$ refer to these channels without indicating the mutations, and the channels not containing the introduced cysteines are referred to as wild-type (WT) channels. The presented results on cysteine mutant channels were obtained after MTS-TAMRA staining, however, application of the dye did not result in significant changes in any of the examined parameters or sterol induced effects (data not shown).

By simultaneously recording ionic currents and fluorescence signals from *Xenopus laevis* oocytes expressing $hK_v1.3$ A309C channels by VCF (**Fig. 2 A**), we obtained current-voltage (I-V) and relative fluorescence change - voltage ($\Delta F/F$-V) curves in the -140 to +40 mV voltage range in 10 mV steps. Cells were depolarized to the test potentials for 250 ms every 30 s from a holding potential of -100 mV. Then, normalized conductance - voltage (G-V) and normalized fluorescence change - voltage (F-V) curves were constructed and fitted with Boltzmann-functions to obtain midpoints ($V_{1/2}$) and slope factors (k) (**Fig. 2 B**). As expected, the midpoint of the F-V curve was hyperpolarized compared to the G-V midpoint ($V_{1/2}$ = -41.1 ± 1.8 mV (n=12) and -15.8 ± 0.5 mV (n=10), respectively) indicating that VSD activation occurs at more negative potentials than pore opening.

Experiments were repeated on cells loaded with cholesterol or 7DHC. Both sterols induced small but significant negative shifts in the G-V curves characterizing pore opening ($V_{1/2}$ = -15.8 ± 0.5 mV (n=10) for control, -21.1 ± 1.5 mV (n=11) for cholesterol and -29.0 ± 1.9 mV (n=12) for 7DHC respectively; p = 0.049, p=0.001) while leaving VSD-related F-V midpoints unaffected ($V_{1/2}$= -41.1 ± 1.8 mV, n=12 for control; -41.5 ± 1.8 mV, n=11 for cholesterol; and -42.1 ± 2.4 mV, n=12 for 7DHC; p = 0.992 and p=0.937 for cholesterol and 7DHC respectively) (**Fig. 2 B,C**). This suggests a direct sterol effect on the pore or the coupling rather than one mediated by VSD activation. F-V slopes were slightly affected, cholesterol induced a significant shallowing of VSD voltage-dependence (k = 15.4 ± 0.4, n=12 for control; 22.2 ± 1.8, n=11 for cholesterol; and 18.7 ± 0.8, n=12 for 7DHC, p=0.002 and p=0.099 for cholesterol and 7DHC respectively) (**Fig. 2 B**).

$K_v1.3$ shows steady-state inactivation (SSI) when held at depolarized potentials, which manifests in decreased peak current during a subsequent strong depolarizing pulse. $K_v1.3$ 309C steady-state inactivation curves showed a similar tendency to G-V curves, being left-shifted by sterols, although only the shift by 7DHC was significant (**Suppl. 2**).

3.2 Sterol effects on voltage-dependent steady-state parameters of $K_v10.1$

In wild-type $K_v10.1$ channels expressed in oocytes we observed similar sterol effects as in $K_v1.3$: reduction of current amplitude, slowing of activation kinetics and a right-shift in the G-V curve (**Suppl. 3**). These results are consistent with previous data examining the effects of cholesterol extraction on wild-type $K_v10.1$ [27].

For studying VSD motions in $K_v10.1$ we used the L322C mutant described earlier [58], but applied MTS-TAMRA for labeling instead of TMR-maleimide. This combination yielded robust multi-phasic voltage-dependent fluorescence signals (**Fig. 2 D**) and did not alter channel gating

significantly (**Fig. 2 D-F, 3C and Suppl. 3**). I-V and ΔF/F-V curves were recorded during depolarizing pulses ranging from -180 to +60 mV in 10 mV steps lasting 800 ms. Pulses were applied every 10 s from a holding potential of -100 mV. In agreement with earlier results, VSD activation in K_v10.1 occurs at very negative potentials (F-V $V_{1/2}$ = -113.6 ± 1.9 mV; n=9), while the pore opens in a similar voltage range as K_v1.3 (G-V $V_{1/2}$ = -25.8 ± 2.1 mV; n=8) (**Fig. 2 D, E**). Therefore, the voltage gap between VSD activation and pore opening is much wider in K_v10.1 than in K_v1.3 indicating a looser coupling between the two functional domains. The effect of sterols on K_v10.1 was very similar to K_v1.3, as both cholesterol and 7DHC induced significant hyperpolarizing shifts in the G-V curve ($V_{1/2}$ = -25.8 ± 1.8 mV (n=8) for control, -33.2 ± 1.8 mV (n=8) for cholesterol and -38.2 ± 2.2 mV (n=9) for 7DHC; p = 0.043 and p=0.002 for cholesterol and 7DHC respectively), but neither had any effect on the midpoint or the slope of the F-V relationship ($V_{1/2}$ = -113.6 ± 1.9 mV (n=9) for control, -113.5 ± 0.6 mV (n=9) for cholesterol and -114.0 ± 1.6 mV (n=8) for 7DHC; p = 0.999 and p= 0.981 for cholesterol and 7DHC respectively) (**F**). Thus, just like in K_v1.3 pore opening, but not VSD activation is affected by sterol loading in K_v10.1.

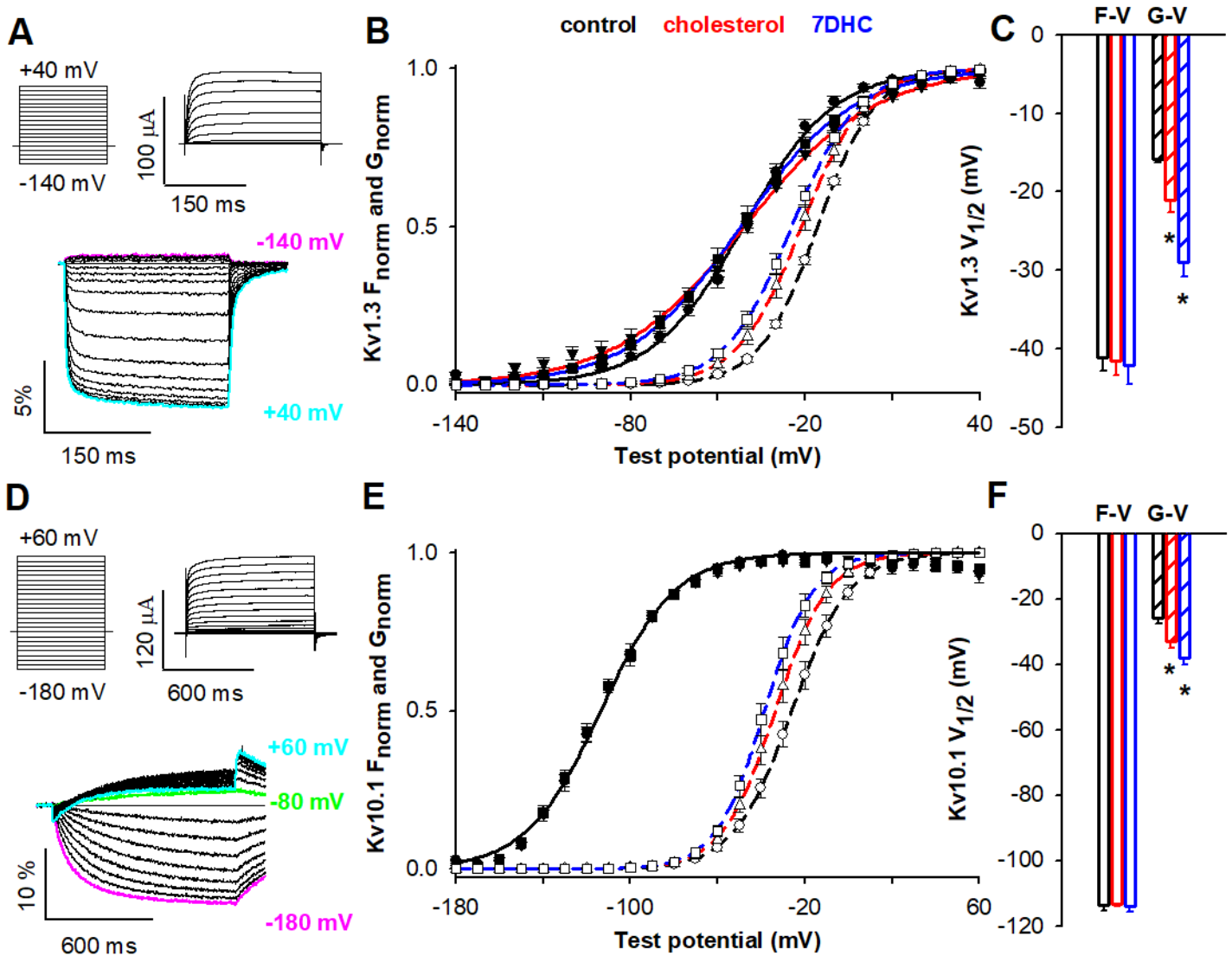

Fig. 2 Effects of sterol loading on voltage-dependent steady-state gating parameters of cysteine mutant K_v1.3 and K_v10.1 channels

To determine steady-state activation of fluorescent signals (ΔF/F) and ionic currents of K_v1.3 (**A**) and K_v10.1 channels (**D**), oocytes were held at −100 mV and depolarized to test potentials ranging from −140 to +40 mV or -180 to +60 mV in steps of 10 mV every 30 or 10 s. The duration of depolarizing pulses was 250 or 800 ms. Voltage protocols (top left plots) and evoked currents (top right plots) are shown in panels (**A**) and (**D**). K_v1.3 channels exhibit a monophasic, while K_v10.1 channels a biphasic fluorescent signal when labeled with MTS-TAMRA, bottom plots of panel (**A**) and (**D**). The superimposed solid (F_{norm}-V) and dashed (G_{norm}-V) lines show best fit Boltzmann functions to the F_{norm}-V (filled symbols) and G_{norm}-V (empty symbols) data points (**B**,**E**). In the case of the F_{norm}-V curves of K_v10.1 all three best fit lines completely overlap. Panel (**C**) and (**F**) show the average $V_{1/2}$ values for K_v1.3 and K_v10.1. Empty columns represent the midpoint of the F_{norm}-V curves, while dashed columns indicate the $V_{1/2}$ values for G_{norm}-V curves. Cholesterol (red) and 7DHC (blue) loading led to significant (*) left shifts in G_{norm}-V curves for both ion channels, while no changes in the $V_{1/2}$ of F_{norm}-V curves were observed (n=8-12).

3.3 Sterol effects on VSD and current activation kinetics

Next the effect of sterol loading on VSD activation and channel opening kinetics was assessed (**Fig. 3**). $K_v1.3$ current activation kinetics, well fit by a single exponential function, were significantly slowed by both cholesterol and 7DHC loading as indicated by the time constants ($p<0.05$ at all voltages) and shown by normalized current traces (**Fig. 3 A inset**). Fluorescence signals had a fast component accounting for the majority (> 85%) of the amplitude and a smaller slow component. In contrast to current kinetics, there was no change in either of the time constants of double exponential fits to VSD activation kinetics in response to sterol loading (**Fig. 3 B**). Furthermore, no significant changes were observed in the ratios of the amplitudes of the time constants due to sterol loading (data not shown).

Activation of $K_v10.1$ currents is known to be modulated by the prepulse holding potential and the external Mg^{2+} concentration, which can result in complex sigmoid kinetics. For the comparability of sterol effects on activation kinetics, we omitted the initial lag phase of the current from the fitting and characterized the rise of the current by single exponentials under all conditions as has been described by others [58,59]. Both cholesterol and 7DHC loading increased current activation time constants, especially at stronger depolarizations, indicating slower pore opening (**Fig. 3 C**). Next, the effect of sterols on VSD kinetics was assessed in the -180 to +60 mV range. Fluorescence signals representing backward VSD transitions to deeper closed states at hyperpolarized potentials had two strongly voltage-dependent kinetic components, neither of which was significantly affected by sterols (**Fig. 3 D**). Depolarizing pulses produced biphasic signals with two components of opposing polarities. The fast component became more prominent with increasing depolarization (**Fig. 2D, bottom plot)** and is likely to represent a VSD transition strongly linked to pore opening based on its voltage range and kinetics. The time constant of the slow component showed marked voltage-dependence and was unaffected by sterol treatment, while the fast component was very weakly voltage-dependent and was significantly slowed by both cholesterol and 7DHC (**Fig. 3 D**,**E**). These observations suggest that VSD transitions between deep closed states are unaltered by sterols, but conformational changes associated with pore opening are slowed.

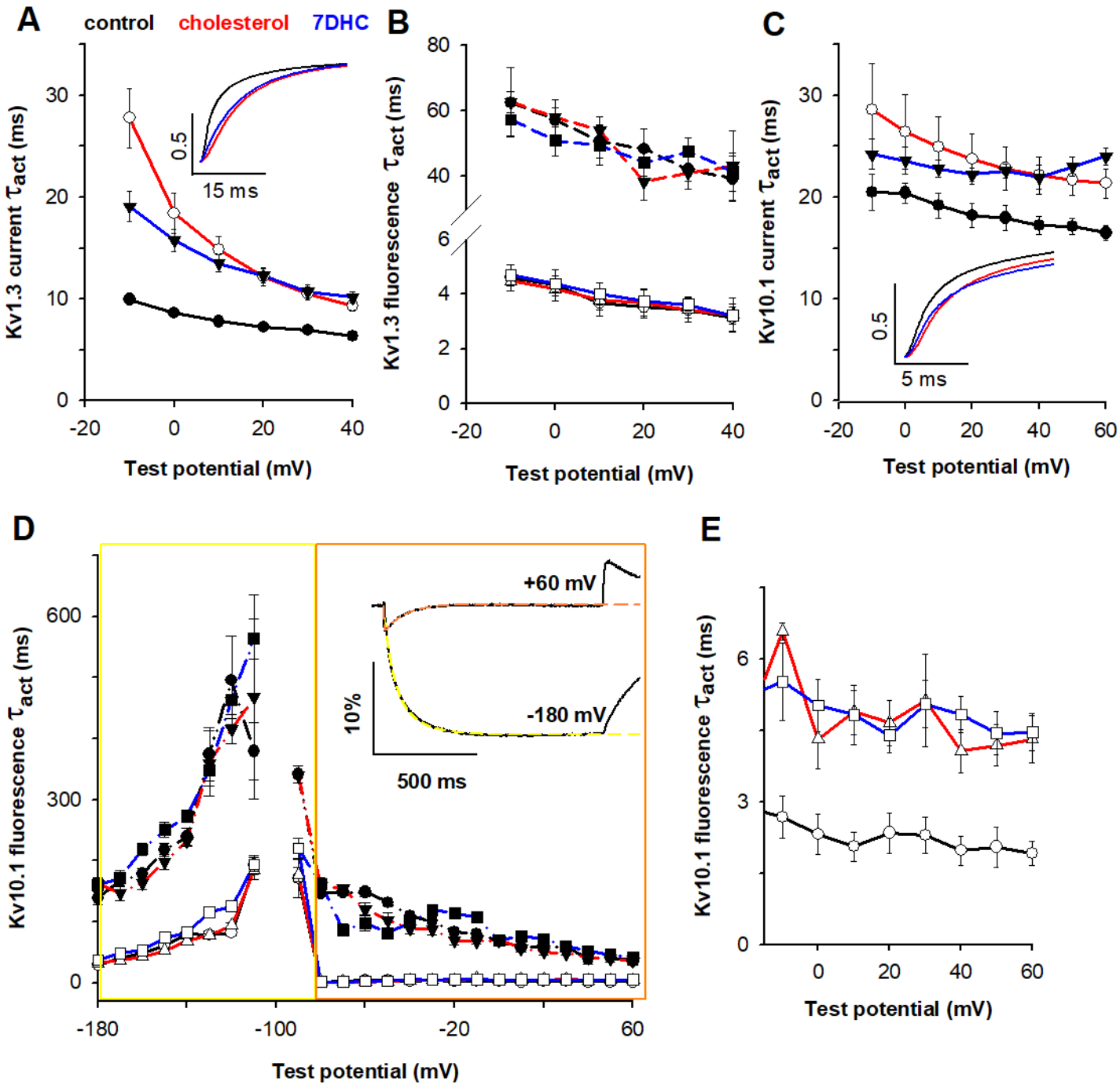

Fig. 3 Effects of sterol loading on current and VSD activation kinetics

When examining kinetic parameters of the $K_v1.3$ and $K_v10.1$ currents and fluorescent signals the same protocols were applied as described in Fig.1. The activation time constants (τ_{act}) of ionic currents were fitted by single exponentials (**A**,**C**), while for fluorescent signals two exponential fitting was used (**B**,**D**). Insets in panels (**A**) and (**C**) show normalized current traces from control (black), cholesterol- (red) and 7DHC-loaded (blue) cells. (**A**) $K_v1.3$ current activation time constants (n=7-11), and (**B**) fast (empty symbols) and slow (filled symbols) fluorescence signal activation time constants (n=4-8) are shown. (**C**)

K_v10.1 current activation time constants (n=4-8). (**D**) Fast (empty symbols) and slow (filled symbols) time constants of the fluorescence signals when stepping to the test potentials from -100 mV. The inset shows best two-exponential fits to fluorescence signals recorded at hyperpolarized (-180 to -110 mV, yellow) and depolarized (-90 to +60 mV, orange) voltages in K_v10.1. (**E**) The fast time constant in the depolarized voltage range shown on expanded scales for control (black), cholesterol- (red) or 7DHC-loaded (blue) cells. (n=5-10).

A characteristic feature of K_v10.1 channels is the Cole-Moore shift, which is apparent as altered current activation kinetics when depolarization occurs from different holding potentials [60]. When channels are activated from very negative potentials they must traverse multiple closed states before opening, a process structurally related to the interaction of the VSD and the PAS domain [45]. Consequently, current activation is sigmoid and slow compared to channels being activated from a more positive holding potential (**Fig. 4**). Current activation kinetics during depolarizing pulses to +40 mV were compared from prepulse holding potentials in the -160 to -60 mV range in control and sterol-loaded cells. Time constants in sterol-loaded cells were similar to control at hyperpolarized holding potentials, but were significantly slower when opening took place from the "pre-open" closed states mostly populated at -60 mV. This indicates that the opening transition is slowed by sterols, but the rate-limiting transitions among deep closed states are not.

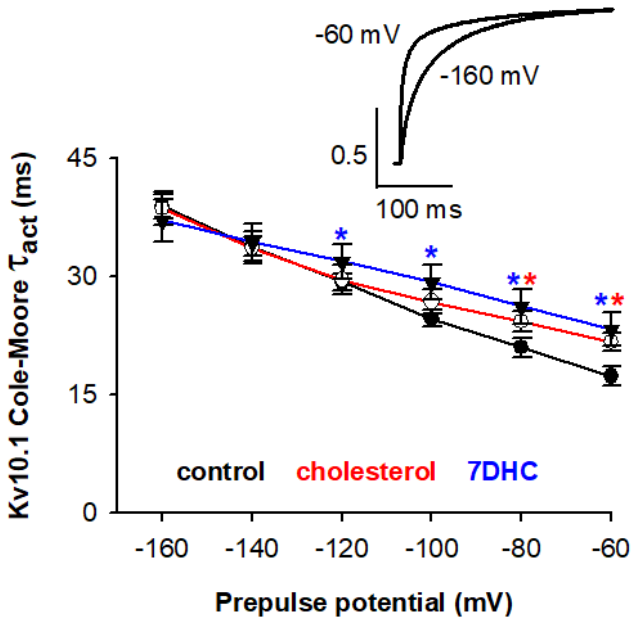

Fig. 4 Modulation of the Cole-Moore shift in K_v10.1 channels by sterols.
To investigate the effect of sterol loading on the Cole-Moore shift of K_v10.1 channel a 500 ms long depolarizing pulse to +40 mV was applied from a 10 s long prepulse holding potential ranging from -160 mV and -60 mVs, in 20 mV increments. Inset demonstrates a representative trace of normalized K_v10.1 currents recorded from prepulse potentials of -160 mV and -60 mV. Currents were fitted by single exponentials excluding the first sigmoidal phase. Cholesterol (red) and 7DHC (blue) loading result in a significant change in τ_{act}s of currents evoked from more positive prepulse potentials (from -120 mV to -60 mV for 7DHC, and from -80 mV to -60 mV for cholesterol) (n=7-8).

3.4 Sterol-induced current reduction

Although current densities could not be compared due to the lack of cell capacitance information, both sterols significantly reduced whole oocyte currents in cells injected by the same amount of RNA and recorded in the same time range following injection for both $K_v1.3$ and $K_v10.1$ channels (**Fig. 5 A**). Amplitudes were reduced to 71.1 ± 8.2 % and 54.0 ± 10.6 % of the control in $K_v1.3$ and to 71.3 ± 8.6 % and 58.5 ± 1.3 % in $K_v10.1$ by cholesterol and 7DHC, respectively (**Fig. 5 B**). To determine the cause of the current reduction, i.e. whether it is due to the reduction of single channel conductance or the open probability, we performed non-stationary noise analysis on excised outside-out membrane patches containing $K_v10.1$ channels. Current fluctuations depend on open probability and single channel conductance, and plotting current variance as a function of current amplitude yields a parabola, whose parameters are suitable to determine these properties of the channels (**Fig. 5 C**). A reduction in the number of active channels may also contribute to current reduction, however, the size of excised patches and consequently the number of channels in the patch varies significantly rendering this value meaningless in assessing the sterol effects. Our analysis indicates that both sterols reduced the single channel conductance (control: 19.73 ± 1.44 pS, n=8; cholesterol: 13.30 ± 1.11 pS, n=6; 7DHC: 14.33 ± 1.04 pS, n=4; p = 0.009, p=0.046), while the open probability was not significantly affected (control: 0.678 ± 0.018 n=8; cholesterol: 0.715 ± 0.035 n=6; 7DHC: 0.573 ± 0.044 n=4; p= 0.628, p=0.067) (**Fig. 5 D**).

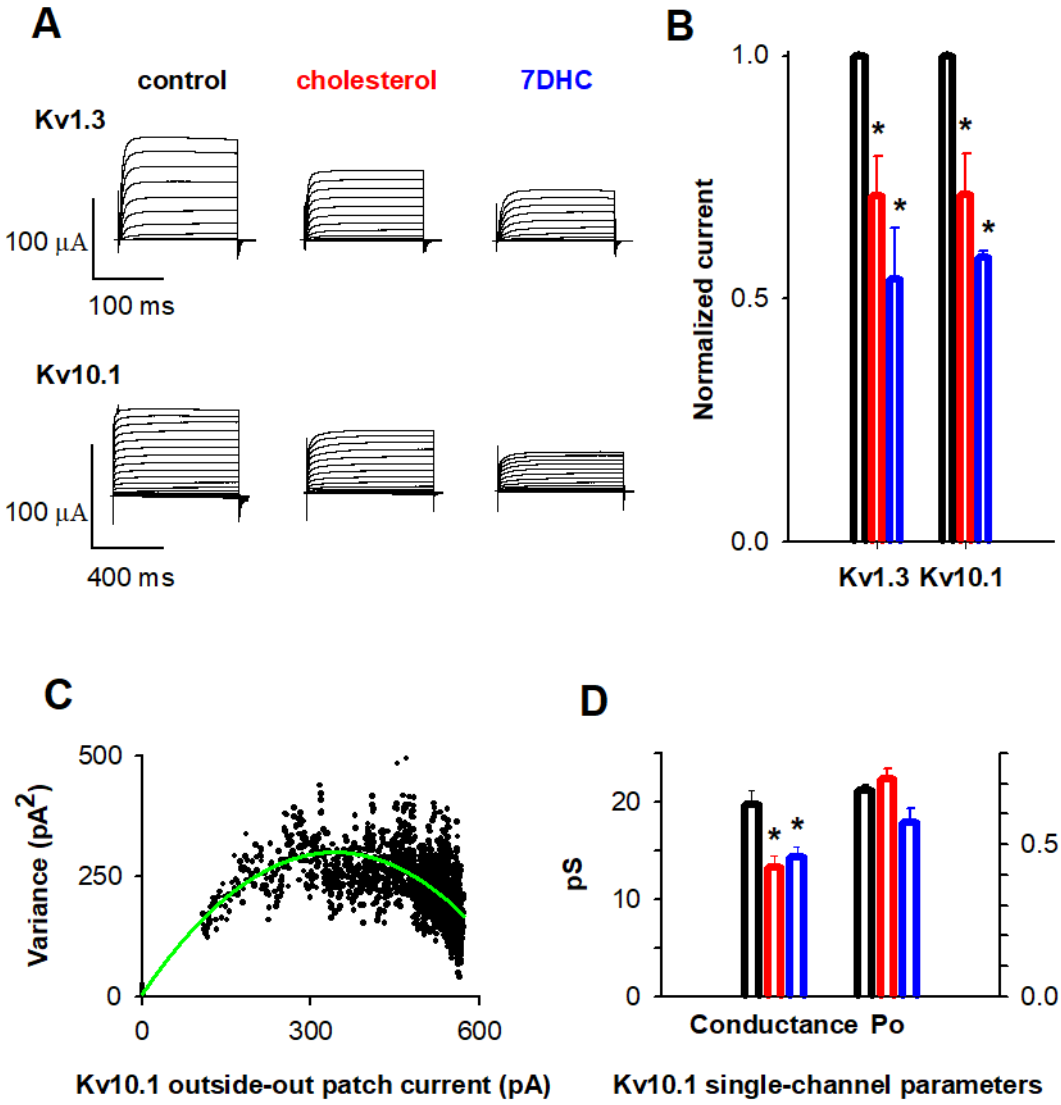

Fig. 5 Effect of sterol loading on whole oocyte current amplitude and single channel parameters

(**A**) Representative current traces obtained from control or sterol-treated oocytes on the same day. (**B**) The daily mean current of cells loaded with cholesterol (red) or 7DHC (blue) normalized to the actual daily mean of control amplitudes (n=3-4 days)**.** Currents were evoked by depolarizing pulses to +40 for $K_V1.3$ or +60 mV for $K_V10.1$. (**C**) Non-stationary current noise analysis on $K_v10.1$ channels expressed in oocytes. During data acquisition outside-out patches pulled from oocytes were held at -100 mV holding potential and a test pulse to +50 mV was applied for 200 ms 200 times. Current variance was plotted against the amplitude at a given time point and the single channel parameters of $K_v10.1$ were determined by fitting a parabola to the data points. (**D**) Single channel conductance and open probability of channels recorded from control (black), cholesterol- (red) and 7DHC-treated (blue) cells (n=5-8). Asterisks (*) indicate significant differences ($p< 0.05$) compared to control samples ($p< 0.05$, ANOVA followed by Tukey's HSD test).

3.5 Raft association of K_v1.3 and K_v10.1

Both K_v1.3 and K_v10.1 were previously shown to be preferentially localized in sphingolipid- and cholesterol-enriched lipid raft microdomains [9,27,61,62]. Since raft localization was found to modulate structural and functional channel properties [9,27,63,64] and cholesterol is an intrinsic major component of rafts [65], channel and raft reorganization upon sterol loading is likely to play a role in the observed sterol effects. To test this hypothesis, we examined the effects of sterol loading on the distribution of K_v1.3 and K_v10.1 between raft and non-raft membrane microdomains by determining the Pearson correlation coefficients between the intensities of antibodies against ion channels and the lipid raft marker choleratoxin B subunit (CTX-B) using confocal and Stimulated Emission Depletion (STED) microscopy, as described previously in detail [54]. Consistent with previous observations, strongly positive Pearson coefficients were found between K_v1.3 or K_v10.1 and CTX-B signals (0.416 ± 0.013, n=27 and 0.298 ± 0.019, n=30, respectively, **Fig. 6 E** and **Suppl. Table 1**). These values were much larger in magnitude than the limits of the 95% confidence intervals of the coefficient assuming no correlation (**Suppl. Table 1**) and were of similar magnitude as obtained in case of positive control samples using two well-established lipid markers, GFP-GPI and CTX-B (0.551 ± 0.020, n=23, **Fig. 6 E** and **Suppl. Table 1**). The co-localization is also clearly demonstrated by our confocal images (**Fig. 6 A-C**) and a representative contour plot showing the correlation between pixelwise intensities (**Fig. 6 D**). In the case of both channels the Pearson coefficients significantly increased in both cholesterol and 7DHC-loaded cells (K_v1.3: 0.492 ± 0.013, n=34, p=0.001 and 0.500 ± 0.015, n=32, p=0.001, K_v10.1: 0.373 ± 0.017, n=29, p=0.010, and 0.395 ± 0.018, n=24, p=0.002, for cholesterol and 7DHC, respectively, **Fig. 6 E** and **Suppl. Table 1**) when observed with confocal laser scanning microscopy. The increased raft localization of Kv1.3 in response to sterols was also confirmed at improved resolution (46-60 nm) provided by STED microscopy. Correlation coefficients were significantly more positive in sterol-loaded samples (cholesterol: 0.361 ± 0.019, n=32, p=0.012, 7DHC: 0.366 ± 0.019, n=28, p=0.010) than in controls (0.274 ± 0.025, n=25) (**Fig. 6 E** and **Suppl. Table 1**). Furthermore, when examining the loading pattern of NBD-cholesterol by confocal microscopy, based on the strong positive Pearson coefficient values the fluorescent cholesterol analog incorporated preferentially into CTX-B labeled lipid raft microdomains (0.234 ± 0.025, n=24), especially into the vicinity of K_v1.3 channels (0.358 ± 0.023, n=24) (**Fig. 6 F** and **Suppl. Table 1)**.

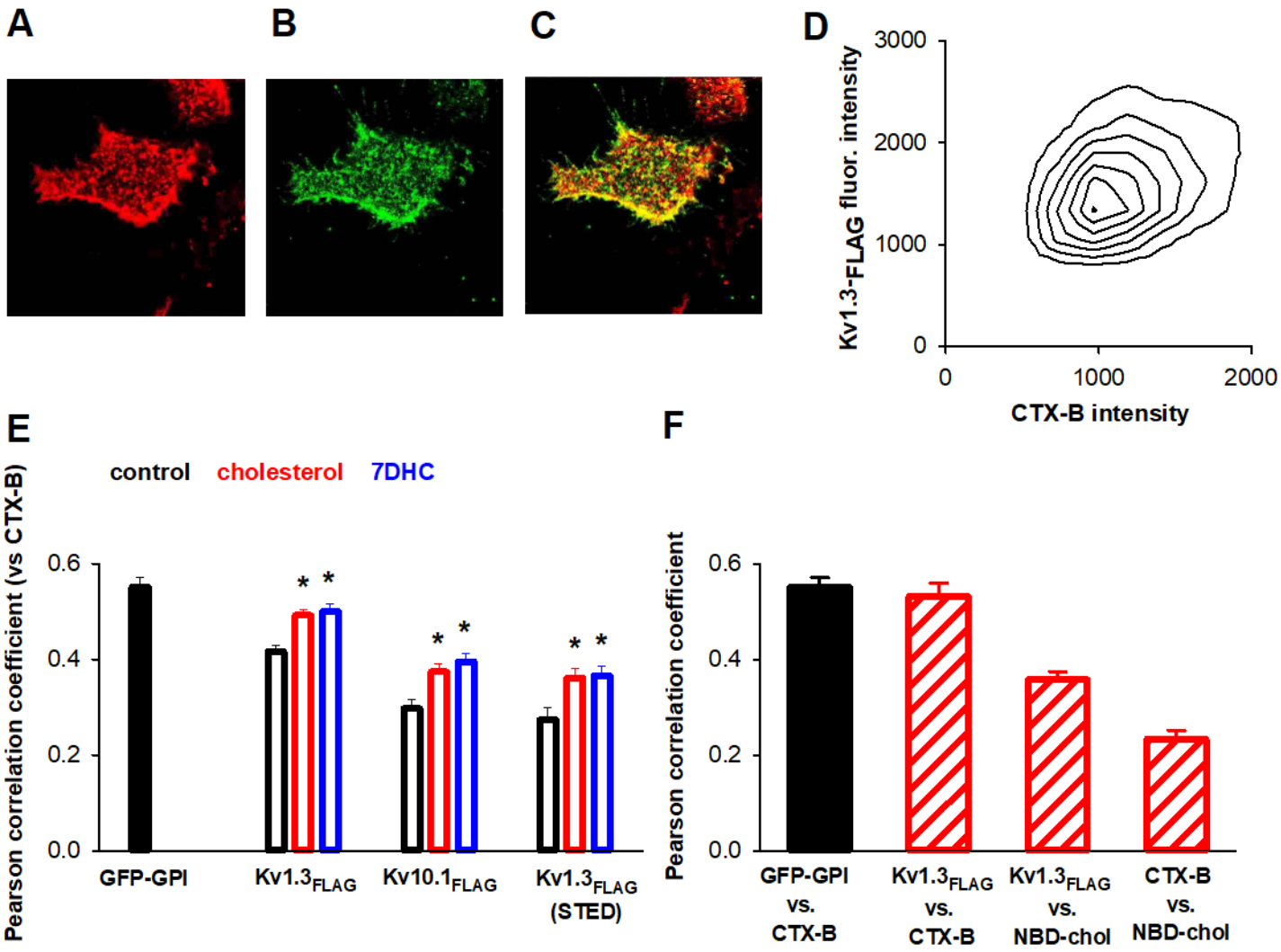

Fig. 6 Effect of sterols on raft partitioning of $K_v1.3$ and $K_v10.1$

After labeling channels and lipid rafts in $K_v1.3$ or $K_v10.1$ expressing sterol-loaded or control HEK-293 cells, images were taken from the flat cell membrane region attached to the coverslip using a confocal laser scanning microscope. Representative images of the distribution of rafts (**A**) and $K_v1.3$ ion channels (**B**) are displayed. Their co-localization is demonstrated by the overlay image (**C**) and the contour plot showing the correlation between pixelwise intensities (**D**). (**E**) Extent of co-localization in control cells and in response to cholesterol (red) or 7DHC (blue) loading, determined quantitatively by the Pearson correlation coefficients between raft and channel signals. Experiments were repeated with $K_v1.3$ at much better (46-60 nm) resolution provided by STED microscopy. (**F**) Pearson coefficients calculated between the indicated labeled molecule pairs in cells loaded with NBD-cholesterol from images recorded by confocal microscopy (n=23-34 cells). Asterisks (*) indicate significant differences ($p< 0.05$) compared to control samples ($p< 0.05$, ANOVA followed by Tukey's HSD test).

4. Discussion

4.1 Sterols do not act via the VSD

The aim of this study was to identify the functional domain of K_v channels, which is targeted by cholesterol to exert its previously documented effects on channel gating. Two K_v channels with different VSD-PD coupling mechanisms were investigated in membranes enriched with cholesterol or 7DHC using MβCD. Voltage-sensitive steady-state and kinetic parameters of the two functional domains were independently tracked by simultaneously measuring the ionic current and fluorescence signal by voltage-clamp fluorometry. We observed similar effects on K_v1.3 and K_v10.1 channels, the minor differences originating from their different gating mechanisms. Several lines of evidence point to the pore domain or the coupling as being the primary direct target of sterol-modulation rather than changes in VSD transitions transmitted to the pore. These are detailed below:

1. The voltage-dependence of pore opening, but not that of VSD activation was shifted along the voltage axis by sterol loading, indicating a change in the energetics of pore opening (**Fig. 2**). This observation also implies a disruption of the coupling between the two functional domains since the G-V and F-V curves are not shifted in a parallel manner. K_v crystal structures and MD simulations indicate that the VSDs are embedded in the membrane, but S4s are mostly shielded away from the lipids, supporting our findings [66]. Although the midpoints of the F-V curves in K_v1.3 were not shifted, the slopes became slightly shallower in response to sterol treatment (the change by 7DHC was not significant) (**Fig. 2 B**). Thus, the energy difference between the resting and activated states of the VSD was not affected, but the apparent gating charge was reduced. This is most likely due to the alteration of the electric field profile across the membrane by cholesterol, as the dipole potential in the membrane was shown to be influenced by cholesterol [67]. MD calculations confirmed that modifying the lipid composition can reshape the electric field profile surrounding the channel and generate detectable changes in the gating charge [66]. Such shallowing was not observed in K_v10.1 (**Fig. 2 E**); control and treated F-V curves completely overlapped. The difference between the two channels may be explained by the observation revealed by analysis of the cryo-electron microscopic (cryo-EM) structure of K_v10.1, which showed that the S4 of K_v10.1 is displaced one 3_{10} helix turn toward the cytosolic side of the membrane compared to the S4 of the K_v1.2-2.1 chimeric channel [45], whose structure better resembles that of K_v1.3. This means that the VSDs of the two channels likely traverse different sections of the membrane during activation and experience different field profiles along the way.

Both in K_v1.3 309C and WT channels the steady-state inactivation curve was shifted by sterols in the same direction as the G-V curves, although these shifts had opposite polarities between the two constructs (**Fig. 2 B**, **C** and **Suppl. 1 D**, **E**). In K_v1.3 C-type inactivation occurs, which involves a rearrangement of the selectivity filter that prevents further conduction of the K^+ ions. This takes place only after pore opening [68] even at holding voltages where macroscopic currents are not apparent and individual channels open with very low probabilities. Thus, sterol enrichment shifting the voltage-dependence of the opening transition is expected to produce such a parallel shift in the SSI curve (**Suppl. 1 E**, **F** and **Suppl. 2**).

2. Pore opening kinetics were slowed, but VSD activation kinetics were mostly unaffected in both channels (**Fig. 3**). Time constants of current activation were significantly longer in the entire examined voltage range for $K_v1.3$ (**Fig. 3 A**), whereas the slowing was mainly apparent above + 10 mV in $K_v10.1$ (**Fig. 3 C**). Only the weakly voltage-dependent fast component of VSD activation in $K_v10.1$, which is linked to pore opening at depolarized potentials was slowed by sterols (**Fig. 3 E**), but not the main voltage-dependent transitions at hyperpolarized potentials. The biphasic activation of the $K_v10.1$ VSD was described previously [58], distinguishing slow transitions at hyperpolarized potentials and faster transitions just preceding the open state. Here we show that the latter, but not the former transitions are modulated by sterol enrichment. The slowing of the fast component of VSD movement may be due to the retrograde action of the pore on the VSD. In $K_v10.1$ coupling is different from $K_v1.3$, the S4-S5 linker is not required for VSD-PD communication, as it was shown that cutting or deleting it completely, did not prevent voltage-gated pore opening. VSD-PD coupling in $K_v10.1$ is assumed to involve direct helix-helix interactions, so it is feasible that a delayed conformational change in the PD is transmitted back to a final conformational rearrangement of the VSD.

3. The Cole-Moore effect in $K_v10.1$ was modulated by sterols: when channels were opened from deep hyperpolarized states, current activation kinetics were not affected, but when opened from pre-open closed states, activation kinetics were significantly slowed (**Fig. 4**),. When channels mostly populate the deep closed states, among which transitions are rate limiting and insensitive to sterols then current activation is not affected. However, when channels mostly start from pre-open closed states from which opening is faster and is sterol-modulated then a slowing of current kinetics is observed. This is compatible with the suggested mechanism for $K_v10.1$ gating based on its cryo-EM structure [45]. According to the model, in the hyperpolarized, or resting state of the VSD, the bottom of S4 pushes on the C-linker, which induces a bend in S6 causing a rotational constriction of the pore, thereby closing it (**Fig. 1 B**). In the depolarized or activated state, S4 moves up and relieves the bend in S6 allowing channel opening. The N-terminus of the PAS domain was suggested to interact with S4 in the resting state, stabilizing it and causing the Cole-Moore effect observed at hyperpolarized potentials. Based on the cryo-EM structure, this interaction is likely to occur in the cytoplasm and not in the membrane, so it is plausible that the VSD conformational changes corresponding to transitions between deep closed states are not affected by the membrane composition. However, the bending of S6 by the bottom of S4 causing pore constriction in the hyperpolarized state and the straightening leading to opening are expected to occur within the membrane being subject to modulation by the surrounding membrane lipids.

4. The current amplitude was reduced by sterols in both WT and mutant channels despite no shifts in the F-V curves and shifts of opposite polarities in the G-V curves (**Fig. 5** and **Suppl. 3 F**). This implies that current reduction must originate from the pore and not the voltage-sensing machinery. Non-stationary noise analysis indicated that sterol-induced current reduction is mainly due to a decrease in single channel conductance and not in open probability. The change in unitary conductance suggests the pore being directly modulated rather than the VSD-PD coupling.

4.2 The role of membrane stress

It is well documented that membrane stretch, for example induced by a patch pipette, has a profound effect on the gating of ion channels, including K_v channels. A simple mechanistic model suggests that membrane stretch favors area / volume expansion of the protein that occurs during the pore opening step, as a result of which channel activation kinetics speed up, voltage-dependence is left-shifted and current amplitude is increased. Cholesterol has long been known to increase lateral stress in the lipid membrane [69], which likely accounts in large part for its effects on embedded channels. In contrast to stretching, this increased lateral stress is expected to favor the closed state of the channel, attenuating its opening kinetics and conductance [8]. In line with this, in most reports, cholesterol enrichment suppressed channel activity, likely by exerting compression on the channel and possibly increasing viscosity in the annular layer. However, such a simple model is insufficient to explain uncorrelated changes in voltage-dependence and gating kinetics. For example, we consistently observed slowing of current activation kinetics by both sterols in all channel constructs (**Fig. 3 A**, **C**; **Suppl. 1 D** and **Suppl. 3 B**), while observing G-V shifts of opposite polarities (**Fig. B**, **E**; **Suppl. 1 B** and **Suppl. 3 D**), indicating that assuming a single forward transition being slowed by cholesterol is inadequate to describe all changes.

4.3 Recruitment to lipid rafts

Different responses of various channels to sterol enrichment may also arise from the relative distribution of the channels and sterols in the membrane. Several channels, including K_v1.3 and K_v10.1 were previously shown to be preferentially localized in sphingolipid- and cholesterol-enriched lipid rafts [9,27,70], while others were shown to be excluded [5]. Consistent with previous studies, we have found strongly positive Pearson coefficients demonstrating the preferential raft localization of both channels, which was further increased by the enrichment of either of the sterols (**Fig. 6** and **Suppl. Table 1**). Here, we provide stronger proof for these observations for K_v1.3 by the much higher resolution of STED microscopy, which confirms the preferential raft localization and its enhancement by sterol loading beyond the power of confocal microscopy. NBD-cholesterol indicated the preferential raft accumulation of cholesterol. Furthermore, positive correlation was found between K_v1.3 and NBD-cholesterol, which was significantly higher than that between the labeled cholesterol and the raft marker. This suggests that exogenously loaded sterols show preference to lipid rafts containing K_v1.3 channels, possibly implying the interaction between cholesterol and K_v1.3.

The local sterol environment around channels is strongly determined by their affinity for rafts, which may be dependent on sterol concentration. K_v1.3 and K_v10.1 responded similarly to sterol-enrichment showing a high preference for raft localization and consequently being prone to sterol-modulation. Given the known fact that raft localization significantly modifies the function of ion channels, our results raise the possibility that the functional effects of sterols on K_v1.3 and K_v10.1 might be at least partially mediated by changes in the distribution of these channels between raft and non-raft microdomains of the cell membrane.

4.4 Cause of current reduction

Whole-cell current increase in response to membrane stretch has been attributed to an increase in open probability in several channel types without a change in single channel conductance [71-74]. For most examined ion channels, including K_v channels, cholesterol enrichment led to a reduction of current amplitude in accord with cholesterol increasing lateral stress. However, current reduction cannot always be accounted for by the reduced open probability induced by stress. The cause of current reduction was found to be variable in different channels: decrease in the open probability [12,75], in the number of active channels [11], or in the single channel conductance [8] have all been described.

In our experiments, current amplitude was reduced and current activation kinetics were slowed in both WT and mutant $K_v1.3$ and $K_v10.1$ channels, regardless of the direction of the G-V shift. This argues against the open probability being modified, as the change in a single transition connected to the open state would cause a parallel shifts in these parameters. Such parallel shifts were shown in midpoint voltage, steepness of G-V curves and maximum P_o in response to membrane stretch, which were all explainable simultaneously by the sole adjustment of the opening transition [76].

A combination of decreased open probability and unitary conductance was observed in BK channels in response to cholesterol enrichment [8]. Compression of the pore by lateral stress without an effect on the selectivity filter was suggested as the mechanism reducing single channel current. Since none of the earlier reports or our own experiments indicated changes in channel selectivity upon sterol enrichment, the selectivity filter is likely to remain intact. Early calculations have shown that the decrease in single channel conductance may be caused by the reduction of the physical dimension of the inner vestibule of the pore, which is located intracellular of the selectivity filter [8,77,78]. The mechanisms raised were a reduced flux rate of ions due to the volume reduction of the vestibule or a change of exposed charges and therefore electric potentials within the pore caused by the distortion. More recent structure-based calculations have confirmed that unitary conductance is very sensitive to small changes in the vestibule diameter [79], so the reduced single channel conductance by slight stress-induced distortion of the pore is a feasible scenario.

4.5 Proposed model

Our results indicate that increased sterol content of the membrane does not affect the voltage-sensing domain, but instead acts directly on the pore. As the mechanism of sterol-induced changes on the pore, we suggest that an important contributing factor is the non-specific increase in lateral stress, which hinders the opening transition and reduces conductance by distorting the inner vestibule. However, as raised earlier [8,80], sterol enrichment may increase the enthalpy of the closed – open transition, but also increase the entropy associated with the conformational change of opening, thus, the sign of the change in free energy, and consequently the direction of the G-V shift, will depend on the relative weight of these terms. An intriguing observation was that in both wild-type $K_v1.3$ and $K_v10.1$ channels sterol-loading caused a right-shift in the G-V curves as opposed to the left-shift caused by sterols in the cysteine-mutant channels used for VCF experiments. At the same time, other effects, such as current reduction and slower current

activation kinetics were similar in WT and mutant channels. Although surprising, such opposite G-V shifts were also observed between WT Shaker and ILT mutant Shaker channels in response to membrane stretch [80], and the effect was confirmed to be mutant-specific and not an artifact. Similar to our results, the analysis of kinetic schemes of Shaker with the ILT triple mutation, which makes the final concerted gating step rate-limiting, indicated that the tension-sensitive step was the final opening of the gate after the movement of the four voltage sensors. Consequently, predicting the effect of membrane stress on channel function is not straightforward, which may explain the many conflicting results in the subject. In addition, specific interactions of sterols with particular channels may tweak the direction of the effects in unexpected directions. In our study, strong influence of specific effects is unlikely, since the two K_v channels with different coupling mechanisms produced very similar responses both to cholesterol and 7DHC. The tendency of particular channels to localize to rafts is also a determinant of overall effects as it influences the local sterol concentration sensed by the channel.

In conclusion, the main target of sterol enrichment on K_v channels is the pore, rather than the voltage-sensing machinery, and the increase in lateral stress by sterols is likely to be the dominating effect modulated by more specific sterol-channel interactions.

Abbreviations

Ala: alanine
7DHC: 7-dehydrocholesterol
CNBHD: cyclic nucleotide binding homology domain
cryo-EM: cryo-electronmicrosopy
CTX: choleratoxin
Cys: cysteine
eag: *ether-à-go-go* family of K_V channels
FLAG: DYKDDDDK epitope
F-V: fluorescence-voltage curve
GFP-GPI: green fluorescent protein-glycosylphosphatidylinositol
G-V: conductance-voltage curve
K_v: voltage-gated potassium channel
MβCD: methyl-beta-cyclodextrin
MTS-TAMRA: methanethiosulfonate-5(6)-carboxytetramethylrhodamine
NBD-cholesterol: 25-[N-[(7-nitro-2-1,3-benzoxadiazol-4-yl)methyl]amino]-27-norcholesterol
PAS: Per-Arnt-Sim domain
PD: pore domain
SSI: steady-state inactivation
STED: stimulated emission depletion microscopy
τ_{act}: activation time constant
TEVCF: two-electrode voltage-clamp fluorometry
TMRM: tetramethylrhodamine maleimide
VSD: voltage-sensor domain

WT: wild-type

Acknowledgements

We thank the expert technical assistance of Adrienn Bagosi. This work was supported by the Hungarian Academy of Sciences project KTIA_NAP_13-2-2015-0009 (Z.V.); János Bolyai Fellowship. (Z.V.); the ÚNKP-18-3-IV-DE-54 New National Excellence Program of the Ministry of Human Capacities (F.Z.); the National Research, Development and Innovation Office (GINOP-2.3.2-15-2016-00044, K120302) (T.K., P.N.) and OTKA K119417 (G.P.).

References

1 Levitan, I., Singh, D. K.and Rosenhouse-Dantsker, A. Cholesterol binding to ion channels. *Frontiers in physiology* **5**, 65, doi:10.3389/fphys.2014.00065 (2014).

2 Liin, S. I., Silvera Ejneby, M., Barro-Soria, R., Skarsfeldt, M. A., Larsson, J. E., Starck Harlin, F., Parkkari, T., Bentzen, B. H., Schmitt, N., Larsson, H. P.and Elinder, F. Polyunsaturated fatty acid analogs act antiarrhythmically on the cardiac IKs channel. *Proc Natl Acad Sci U S A* **112**, 5714-5719, doi:10.1073/pnas.1503488112 (2015).

3 Tobelaim, W. S., Dvir, M., Lebel, G., Cui, M., Buki, T., Peretz, A., Marom, M., Haitin, Y., Logothetis, D. E., Hirsch, J. A.and Attali, B. Ca(2+)-Calmodulin and PIP2 interactions at the proximal C-terminus of Kv7 channels. *Channels (Austin)* **11**, 686-695, doi:10.1080/19336950.2017.1388478 (2017).

4 Levitan, I., Fang, Y., Rosenhouse-Dantsker, A.and Romanenko, V. Cholesterol and ion channels. *Sub-cellular biochemistry* **51**, 509-549, doi:10.1007/978-90-481-8622-8_19 (2010).

5 Martens, J. R., Navarro-Polanco, R., Coppock, E. A., Nishiyama, A., Parshley, L., Grobaski, T. D.and Tamkun, M. M. Differential targeting of Shaker-like potassium channels to lipid rafts. *Journal of Biological Chemistry* **275**, 7443-7446 (2000).

6 Martens, J. R., Sakamoto, N., Sullivan, S. A., Grobaski, T. D.and Tamkun, M. M. Isoform-specific localization of voltage-gated K+ channels to distinct lipid raft populations. Targeting of Kv1.5 to caveolae. *Journal of Biological Chemistry* **276**, 8409-8414 (2001).

7 Bolotina, V., Omelyanenko, V., Heyes, B., Ryan, U.and Bregestovski, P. Variations of membrane cholesterol alter the kinetics of Ca2(+)-dependent K+ channels and membrane fluidity in vascular smooth muscle cells. *Pflugers Arch.* **415**, 262-268 (1989).

8 Chang, H. M., Reitstetter, R., Mason, R. P.and Gruener, R. Attenuation of channel kinetics and conductance by cholesterol: an interpretation using structural stress as a unifying concept. *J Membr.Biol* **143**, 51-63 (1995).

9 Bock, J., Szabo, I., Gamper, N., Adams, C.and Gulbins, E. Ceramide inhibits the potassium channel Kv1.3 by the formation of membrane platforms. *Biochemical and Biophysical Research Communications* **305**, 890-897 (2003).

10 Hajdu, P., Varga, Z., Pieri, C., Panyi, G.and Gaspar, R., Jr. Cholesterol modifies the gating of Kv1.3 in human T lymphocytes. *Pflugers Arch.* **445**, 674-682 (2003).

11 Romanenko, V. G., Fang, Y., Byfield, F., Travis, A. J., Vandenberg, C. A., Rothblat, G. H.and Levitan, I. Cholesterol sensitivity and lipid raft targeting of Kir2.1 channels. *Biophys J* **87**, 3850-3861, doi:10.1529/biophysj.104.043273 (2004).

12 Bukiya, A. N., Belani, J. D., Rychnovsky, S.and Dopico, A. M. Specificity of cholesterol and analogs to modulate BK channels points to direct sterol-channel protein interactions. *J Gen Physiol* **137**, 93-110, doi:10.1085/jgp.201010519 (2011).

13 Chun, Y. S., Shin, S., Kim, Y., Cho, H., Park, M. K., Kim, T. W., Voronov, S. V., Di Paolo, G., Suh, B. C.and Chung, S. Cholesterol modulates ion channels via down-regulation of phosphatidylinositol 4,5-bisphosphate. *Journal of neurochemistry* **112**, 1286-1294, doi:10.1111/j.1471-4159.2009.06545.x (2010).

14 Abi-Char, J., Maguy, A., Coulombe, A., Balse, E., Ratajczak, P., Samuel, J. L., Nattel, S.and Hatem, S. N. Membrane cholesterol modulates Kv1.5 potassium channel distribution and function in rat cardiomyocytes. *J Physiol* **582**, 1205-1217, doi:10.1113/jphysiol.2007.134809 (2007).

15 Lundbaek, J. A., Birn, P., Hansen, A. J., Sogaard, R., Nielsen, C., Girshman, J., Bruno, M. J., Tape, S. E., Egebjerg, J., Greathouse, D. V., Mattice, G. L., Koeppe, R. E., 2ndand Andersen, O. S. Regulation of sodium channel function by bilayer elasticity: the importance of hydrophobic

coupling. Effects of Micelle-forming amphiphiles and cholesterol. *J Gen Physiol* **123**, 599-621, doi:10.1085/jgp.200308996 (2004).

16 Romanenko, V. G., Rothblat, G. H.and Levitan, I. Sensitivity of volume-regulated anion current to cholesterol structural analogues. *J Gen Physiol* **123**, 77-87, doi:10.1085/jgp.200308882 (2004).

17 Krueger, B., Haerteis, S., Yang, L., Hartner, A., Rauh, R., Korbmacher, C.and Diakov, A. Cholesterol depletion of the plasma membrane prevents activation of the epithelial sodium channel (ENaC) by SGK1. *Cell Physiol Biochem* **24**, 605-618, doi:10.1159/000257516 (2009).

18 Peters, M., Katz, B., Lev, S., Zaguri, R., Gutorov, R.and Minke, B. Depletion of Membrane Cholesterol Suppresses Drosophila Transient Receptor Potential-Like (TRPL) Channel Activity. *Current topics in membranes* **80**, 233-254, doi:10.1016/bs.ctm.2017.05.005 (2017).

19 Saghy, E., Payrits, M., Biro-Suto, T., Skoda-Foldes, R., Szanti-Pinter, E., Erostyak, J., Makkai, G., Setalo, G., Jr., Kollar, L., Koszegi, T., Csepregi, R., Szolcsanyi, J., Helyes, Z.and Szoke, E. Carboxamido steroids inhibit the opening properties of Transient Receptor Potential ion channels by lipid raft modulation. *J Lipid Res*, doi:10.1194/jlr.M084723 (2018).

20 Lundbaek, J. A., Birn, P., Girshman, J., Hansen, A. J.and Andersen, O. S. Membrane stiffness and channel function. *Biochemistry* **35**, 3825-3830 (1996).

21 Andersen, O. S., Nielsen, C., Maer, A. M., Lundbaek, J. A., Goulian, M.and Koeppe, R. E. Ion channels as tools to monitor lipid bilayer-membrane protein interactions: gramicidin channels as molecular force transducers. *Methods Enzymol.* **294**, 208-224 (1999).

22 Evans, E.and Needham, D. Physical-Properties of Surfactant Bilayer-Membranes - Thermal Transitions, Elasticity, Rigidity, Cohesion, and Colloidal Interactions. *J Phys Chem-Us* **91**, 4219-4228, doi:Doi 10.1021/J100300a003 (1987).

23 Barbera, N., Ayee, M. A. A., Akpa, B. S.and Levitan, I. Differential Effects of Sterols on Ion Channels: Stereospecific Binding vs Stereospecific Response. *Current topics in membranes* **80**, 25-50, doi:10.1016/bs.ctm.2017.06.001 (2017).

24 Romanenko, V. G., Rothblat, G. H.and Levitan, I. Modulation of endothelial inward-rectifier K+ current by optical isomers of cholesterol. *Biophys J* **83**, 3211-3222, doi:10.1016/S0006-3495(02)75323-X (2002).

25 Simons, K.and Ehehalt, R. Cholesterol, lipid rafts, and disease. *J Clin Invest* **110**, 597-603, doi:10.1172/JCI16390 (2002).

26 Felipe, A., Soler, C.and Comes, N. Kv1.5 in the immune system: the good, the bad, or the ugly? *Frontiers in physiology* **1**, 152, doi:10.3389/fphys.2010.00152 (2010).

27 Jimenez-Garduno, A. M., Mitkovski, M., Alexopoulos, I. K., Sanchez, A., Stuhmer, W., Pardo, L. A.and Ortega, A. KV10.1 K(+)-channel plasma membrane discrete domain partitioning and its functional correlation in neurons. *Biochim Biophys Acta* **1838**, 921-931, doi:10.1016/j.bbamem.2013.11.007 (2014).

28 Klein, U., Gimpl, G.and Fahrenholz, F. Alteration of the myometrial plasma membrane cholesterol content with beta-cyclodextrin modulates the binding affinity of the oxytocin receptor. *Biochemistry* **34**, 13784-13793 (1995).

29 Zidovetzki, R.and Levitan, I. Use of cyclodextrins to manipulate plasma membrane cholesterol content: evidence, misconceptions and control strategies. *Biochim Biophys Acta* **1768**, 1311-1324, doi:10.1016/j.bbamem.2007.03.026 (2007).

30 Mahammad, S.and Parmryd, I. Cholesterol homeostasis in T cells. Methyl-beta-cyclodextrin treatment results in equal loss of cholesterol from Triton X-100 soluble and insoluble fractions. *Biochim Biophys Acta* **1778**, 1251-1258, doi:10.1016/j.bbamem.2008.02.010 (2008).

31 Wong, W.and Schlichter, L. C. Differential recruitment of Kv1.4 and Kv4.2 to lipid rafts by PSD-95. *J Biol Chem* **279**, 444-452, doi:10.1074/jbc.M304675200 (2004).

32 O'Connell, K. M.and Tamkun, M. M. Targeting of voltage-gated potassium channel isoforms to distinct cell surface microdomains. *Journal of cell science* **118**, 2155-2166, doi:10.1242/jcs.02348 (2005).

33 O'Connell, K. M., Whitesell, J. D.and Tamkun, M. M. Localization and mobility of the delayed-rectifer K+ channel Kv2.1 in adult cardiomyocytes. *Am J Physiol Heart Circ Physiol* **294**, H229-237, doi:10.1152/ajpheart.01038.2007 (2008).

34 Balajthy, A., Hajdu, P., Panyi, G.and Varga, Z. Sterol Regulation of Voltage-Gated K(+) Channels. *Current topics in membranes* **80**, 255-292, doi:10.1016/bs.ctm.2017.05.006 (2017).

35 Alexander, S. P., Striessnig, J., Kelly, E., Marrion, N. V., Peters, J. A., Faccenda, E., Harding, S. D., Pawson, A. J., Sharman, J. L., Southan, C., Davies, J. A.and Collaborators, C. THE CONCISE GUIDE TO PHARMACOLOGY 2017/18: Voltage-gated ion channels. *Br J Pharmacol* **174 Suppl 1**, S160-S194, doi:10.1111/bph.13884 (2017).

36 Matteson, D. R.and Deutsch, C. K channels in T lymphocytes: a patch clamp study using monoclonal antibody adhesion. *Nature* **307**, 468-471 (1984).

37 Pardo, L. A.and Stuhmer, W. Eag1: an emerging oncological target. *Cancer research* **68**, 1611-1613, doi:10.1158/0008-5472.CAN-07-5710 (2008).

38 MacKinnon, R. Determination of the subunit stoichiometry of a voltage-activated potassium channel. *Nature* **350**, 232-235 (1991).

39 Doyle, D. A., Morais, C. J., Pfuetzner, R. A., Kuo, A., Gulbis, J. M., Cohen, S. L., Chait, B. T.and MacKinnon, R. The structure of the potassium channel: molecular basis of K+ conduction and selectivity. *Science* **280**, 69-77 (1998).

40 Long, S. B., Campbell, E. B.and MacKinnon, R. Crystal structure of a mammalian voltage-dependent Shaker family K+ channel. *Science* **309**, 897-903 (2005).

41 Catterall, W. A. Ion channel voltage sensors: structure, function, and pathophysiology. *Neuron* **67**, 915-928, doi:10.1016/j.neuron.2010.08.021 (2010).

42 Noda, M., Shimizu, S., Tanabe, T., Takai, T., Kayano, T., Ikeda, T., Takahashi, H., Nakayama, H., Kanaoka, Y., Minamino, N.and et al. Primary structure of Electrophorus electricus sodium channel deduced from cDNA sequence. *Nature* **312**, 121-127 (1984).

43 Long, S. B., Campbell, E. B.and MacKinnon, R. Voltage sensor of Kv1.2: structural basis of electromechanical coupling. *Science* **309**, 903-908 (2005).

44 Tomczak, A. P., Fernandez-Trillo, J., Bharill, S., Papp, F., Panyi, G., Stuhmer, W., Isacoff, E. Y.and Pardo, L. A. A new mechanism of voltage-dependent gating exposed by KV10.1 channels interrupted between voltage sensor and pore. *J Gen Physiol* **149**, 577-593, doi:10.1085/jgp.201611742 (2017).

45 Whicher, J. R.and MacKinnon, R. Structure of the voltage-gated K(+) channel Eag1 reveals an alternative voltage sensing mechanism. *Science* **353**, 664-669, doi:10.1126/science.aaf8070 (2016).

46 Van Slyke, A. C., Rezazadeh, S., Snopkowski, M., Shi, P., Allard, C. R.and Claydon, T. W. Mutations within the S4-S5 linker alter voltage sensor constraints in hERG K+ channels. *Biophys J* **99**, 2841-2852, doi:10.1016/j.bpj.2010.08.030 (2010).

47 Lorinczi, E., Gomez-Posada, J. C., de la Pena, P., Tomczak, A. P., Fernandez-Trillo, J., Leipscher, U., Stuhmer, W., Barros, F.and Pardo, L. A. Voltage-dependent gating of KCNH potassium channels lacking a covalent link between voltage-sensing and pore domains. *Nature communications* **6**, 6672, doi:10.1038/ncomms7672 (2015).

48 Balijepalli, R. C., Delisle, B. P., Balijepalli, S. Y., Foell, J. D., Slind, J. K., Kamp, T. J.and January, C. T. Kv11.1 (ERG1) K+ channels localize in cholesterol and sphingolipid enriched membranes and are modulated by membrane cholesterol. *Channels (Austin)* **1**, 263-272 (2007).

49 Vicente, R., Villalonga, N., Calvo, M., Escalada, A., Solsona, C., Soler, C., Tamkun, M. M.and Felipe, A. Kv1.5 association modifies Kv1.3 traffic and membrane localization. *J Biol Chem* **283**, 8756-8764, doi:10.1074/jbc.M708223200 (2008).

50 Martinez-Marmol, R., Villalonga, N., Sole, L., Vicente, R., Tamkun, M. M., Soler, C.and Felipe, A. Multiple Kv1.5 targeting to membrane surface microdomains. *J Cell Physiol* **217**, 667-673, doi:10.1002/jcp.21538 (2008).

51 Pottosin, II, Valencia-Cruz, G., Bonales-Alatorre, E., Shabala, S. N.and Dobrovinskaya, O. R. Methyl-beta-cyclodextrin reversibly alters the gating of lipid rafts-associated Kv1.3 channels in Jurkat T lymphocytes. *Pflugers Arch* **454**, 235-244, doi:10.1007/s00424-007-0208-4 (2007).

52 Balajthy, A., Somodi, S., Petho, Z., Peter, M., Varga, Z., Szabo, G. P., Paragh, G., Vigh, L., Panyi, G.and Hajdu, P. 7DHC-induced changes of Kv1.3 operation contributes to modified T cell function in Smith-Lemli-Opitz syndrome. *Pflugers Arch* **468**, 1403-1418, doi:10.1007/s00424-016-1851-4 (2016).

53 Porter, F. D. Smith-Lemli-Opitz syndrome: pathogenesis, diagnosis and management. *European journal of human genetics : EJHG* **16**, 535-541, doi:10.1038/ejhg.2008.10 (2008).

54 Kovacs, T., Batta, G., Zakany, F., Szollosi, J.and Nagy, P. The dipole potential correlates with lipid raft markers in the plasma membrane of living cells. *J Lipid Res* **58**, 1681-1691, doi:10.1194/jlr.M077339 (2017).

55 Alvarez, O., Gonzalez, C.and Latorre, R. Counting channels: a tutorial guide on ion channel fluctuation analysis. *Advances in physiology education* **26**, 327-341, doi:10.1152/advan.00006.2002 (2002).

56 Kovacs, T., Batta, G., Hajdu, T., Szabo, A., Varadi, T., Zakany, F., Csomos, I., Szollosi, J.and Nagy, P. The Dipole Potential Modifies the Clustering and Ligand Binding Affinity of ErbB Proteins and Their Signaling Efficiency. *Sci Rep* **6**, 35850, doi:10.1038/srep35850 (2016).

57 Costes, S. V., Daelemans, D., Cho, E. H., Dobbin, Z., Pavlakis, G.and Lockett, S. Automatic and quantitative measurement of protein-protein colocalization in live cells. *Biophysical journal* **86**, 3993-4003, doi:10.1529/biophysj.103.038422 (2004).

58 Bannister, J. P., Chanda, B., Bezanilla, F.and Papazian, D. M. Optical detection of rate-determining ion-modulated conformational changes of the ether-a-go-go K+ channel voltage sensor. *Proc Natl Acad Sci U S A* **102**, 18718-18723, doi:10.1073/pnas.0505766102 (2005).

59 Terlau, H., Ludwig, J., Steffan, R., Pongs, O., Stuhmer, W.and Heinemann, S. H. Extracellular Mg2+ regulates activation of rat eag potassium channel. *Pflugers Arch* **432**, 301-312 (1996).

60 Terlau, H., Heinemann, S. H., Stuhmer, W., Pongs, O.and Ludwig, J. Amino terminal-dependent gating of the potassium channel rat eag is compensated by a mutation in the S4 segment. *J Physiol* **502 (Pt 3)**, 537-543 (1997).

61 Panyi, G., Vamosi, G., Bacso, Z., Bagdany, M., Bodnar, A., Varga, Z., Gaspar, R., Matyus, L.and Damjanovich, S. Kv1.3 potassium channels are localized in the immunological synapse formed between cytotoxic and target cells. *Proc.Natl.Acad.Sci.U.S.A* **101**, 1285-1290 (2004).

62 Martinez-Marmol, R., Styrczewska, K., Perez-Verdaguer, M., Vallejo-Gracia, A., Comes, N., Sorkin, A.and Felipe, A. Ubiquitination mediates Kv1.3 endocytosis as a mechanism for protein kinase C-dependent modulation. *Sci Rep* **7**, 42395, doi:10.1038/srep42395 (2017).

63 Nicolaou, S. A., Neumeier, L., Steckly, A., Kucher, V., Takimoto, K.and Conforti, L. Localization of Kv1.3 channels in the immunological synapse modulates the calcium response to antigen stimulation in T lymphocytes. *J Immunol* **183**, 6296-6302, doi:10.4049/jimmunol.0900613 (2009).

64 Izsepi, E., Himer, L., Szilagyi, O., Hajdu, P., Panyi, G., Laszlo, G.and Matko, J. Membrane microdomain organization, calcium signal, and NFAT activation as an important axis in polarized

Th cell function. *Cytometry. Part A : the journal of the International Society for Analytical Cytology* **83**, 185-196, doi:10.1002/cyto.a.22234 (2013).

65 Sezgin, E., Levental, I., Mayor, S.and Eggeling, C. The mystery of membrane organization: composition, regulation and roles of lipid rafts. *Nature reviews. Molecular cell biology* **18**, 361-374, doi:10.1038/nrm.2017.16 (2017).

66 Kasimova, M. A., Tarek, M., Shaytan, A. K., Shaitan, K. V.and Delemotte, L. Voltage-gated ion channel modulation by lipids: insights from molecular dynamics simulations. *Biochim Biophys Acta* **1838**, 1322-1331, doi:10.1016/j.bbamem.2014.01.024 (2014).

67 Starke-Peterkovic, T., Turner, N., Vitha, M. F., Waller, M. P., Hibbs, D. E.and Clarke, R. J. Cholesterol effect on the dipole potential of lipid membranes. *Biophys J* **90**, 4060-4070, doi:10.1529/biophysj.105.074666 (2006).

68 Cuello, L. G., Jogini, V., Cortes, D. M., Pan, A. C., Gagnon, D. G., Dalmas, O., Cordero-Morales, J. F., Chakrapani, S., Roux, B.and Perozo, E. Structural basis for the coupling between activation and inactivation gates in K(+) channels. *Nature* **466**, 272-275, doi:10.1038/nature09136 (2010).

69 Needham, D.and Nunn, R. S. Elastic deformation and failure of lipid bilayer membranes containing cholesterol. *Biophys J* **58**, 997-1009, doi:10.1016/S0006-3495(90)82444-9 (1990).

70 Vamosi, G., Bacso, Z., Bodnar, A., Bagdany, M., Varga, Z., Gaspar, R., Matyus, L., Damjanovich, S.and Panyi, G. Kv1.3 potassium channels are localized in the immunological synapse formed between cytotoxic and target cells. *Biophys J* **86**, 540A-540A (2004).

71 Patel, A. J., Lazdunski, M.and Honore, E. Lipid and mechano-gated 2P domain K(+) channels. *Current opinion in cell biology* **13**, 422-428 (2001).

72 Clausen, M. V., Jarerattanachat, V., Carpenter, E. P., Sansom, M. S. P.and Tucker, S. J. Asymmetric mechanosensitivity in a eukaryotic ion channel. *Proc Natl Acad Sci U S A* **114**, E8343-E8351, doi:10.1073/pnas.1708990114 (2017).

73 Loukin, S., Zhou, X., Su, Z., Saimi, Y.and Kung, C. Wild-type and brachyolmia-causing mutant TRPV4 channels respond directly to stretch force. *J Biol Chem* **285**, 27176-27181, doi:10.1074/jbc.M110.143370 (2010).

74 Anishkin, A., Loukin, S. H., Teng, J.and Kung, C. Feeling the hidden mechanical forces in lipid bilayer is an original sense. *Proc Natl Acad Sci U S A* **111**, 7898-7905, doi:10.1073/pnas.1313364111 (2014).

75 Toselli, M., Biella, G., Taglietti, V., Cazzaniga, E.and Parenti, M. Caveolin-1 expression and membrane cholesterol content modulate N-type calcium channel activity in NG108-15 cells. *Biophys J* **89**, 2443-2457, doi:10.1529/biophysj.105.065623 (2005).

76 Schmidt, D.and MacKinnon, R. Voltage-dependent K+ channel gating and voltage sensor toxin sensitivity depend on the mechanical state of the lipid membrane. *Proc Natl Acad Sci U S A* **105**, 19276-19281, doi:10.1073/pnas.0810187105 (2008).

77 Latorre, R.and Miller, C. Conduction and selectivity in potassium channels. *The Journal of membrane biology* **71**, 11-30 (1983).

78 Dani, J. A. Ion-channel entrances influence permeation. Net charge, size, shape, and binding considerations. *Biophys J* **49**, 607-618, doi:10.1016/S0006-3495(86)83688-8 (1986).

79 Naranjo, D., Moldenhauer, H., Pincuntureo, M.and Diaz-Franulic, I. Pore size matters for potassium channel conductance. *J Gen Physiol* **148**, 277-291, doi:10.1085/jgp.201611625 (2016).

80 Laitko, U., Juranka, P. F.and Morris, C. E. Membrane stretch slows the concerted step prior to opening in a Kv channel. *J Gen Physiol* **127**, 687-701, doi:10.1085/jgp.200509394 (2006).

Highlights

- Sterols alter pore opening, but not voltage-sensor activation of K_v channels
- Sterol loading slows current kinetics, but not voltage-sensor kinetics
- Sterols reduce single channel conductance without influencing open probability
- Sterols change raft vs non-raft distribution of K_v1.3 and K_v10.1
- Sterols directly target the pore rather than the VSD of K_v channels